Research Article | Vol. 25, No. 16 | 7 Aug 2017 | OPTICS EXPRESS 19298
Optics EXPRESS

# Nanoscale liquid crystal polymer Bragg polarization gratings

XIAO XIANG,[1] JIHWAN KIM,[2] RAVI KOMANDURI,[2] AND MICHAEL J. ESCUTI[2,*]

[1]*Department of Physics, North Carolina State University, Raleigh, NC 27695, USA*
[2]*Department of Electrical and Computer Engineering, Raleigh, NC 27695, USA*
[*]*mjescuti@ncsu.edu*
*http://go.ncsu.edu/gpl*

**Abstract:** We experimentally demonstrate nearly ideal liquid crystal (LC) polymer Bragg polarization gratings (PGs) operating at a visible wavelength of 450 nm and with a sub-wavelength period of 335 nm. Bragg PGs employ the geometric (Pancharatnam-Berry) phase, and have many properties fundamentally different than their isotropic analog. However, until now Bragg PGs with nanoscale periods (e.g., < 800 nm) have not been realized. Using photo-alignment polymers and high-birefringence LC materials, we employ multiple thin sublayers to overcome the critical thickness threshold, and use chiral dopants to induce a helical twist that effectively generates a slanted grating. These LC polymer Bragg PGs manifest 85-99% first-order efficiency, 19-29° field-of-view, $Q \approx 17$, 200 nm spectral bandwidth, 84° deflection angle in air (in one case), and efficient waveguide-coupling (in another case). Compared to surface-relief and volume-holographic gratings, they show high efficiency with larger angular/spectral bandwidths and potentially simpler fabrication. These nanoscale Bragg PGs manifest a $6\pi$ rad/$\mu$m phase gradient, the largest reported for a geometric-phase hologram while maintaining a first-order efficiency near 100%.



**OCIS codes:** (050.1950) Diffraction gratings; (050.6624) Subwavelength structures; (160.3710) Liquid crystals; (310.6845) Thin film devices and applications.

## References and links

1. L. Nikolova and T. Todorov, "Diffraction efficiency and selectivity of polarization holographic recording," Opt. Acta **31**(5), 579–588 (1984).
2. F. Gori, "Measuring Stokes parameters by means of a polarization grating," Opt. Lett. **24**(9), 584–586 (1999).
3. Z. Bomzon, G. Biener, V. Kleiner, and E. Hasman, "Space-variant Pancharatnam-Berry phase optical elements with computer-generated subwavelength gratings," Opt. Lett. **27**(13), 1141–1143 (2002).
4. M. Ishiguro, D. Sato, A. Shishido, and T. Ikeda, "Bragg-type polarization gratings formed in thick polymer films Containing Azobenzene and Tolane Moieties," Langmuir **23**(1), 332–338 (2007).
5. J. Tervo, V. Kettunen, M. Honkanen, and J. Turunen, "Design of space-variant diffractive polarization elements," J. Opt. Soc. Am. A **20**(2), 282–289 (2003).
6. A. Niv, G. Biener, V. Kleiner, and E. Hasman, "Formation of complex wavefronts by use of quasi-periodic subwavelength structures," Proc. SPIE **5347**, 126–136 (2004).
7. G. Zheng, H. Muhlenbernd, M. Kenney, G. Li, T. Zentgraf, and S. Zhang, "Metasurface holograms reaching 80% efficiency," Nat. Nanotechnol. **10**, 308–312 (2015).
8. G. Crawford, J. Eakin, M. Radcliffe, A. Callan-Jones, and R. Pelcovits, "Liquid-crystal diffraction gratings using polarization holography alignment techniques," J. Appl. Phys. **98**, 123102 (2005).
9. M. J. Escuti, C. Oh, C. Sanchez, C. Bastiaansen, and D. Broer, "Simplified spectropolarimetry using reactive mesogen polarization gratings," Proc. SPIE **6302**, 630207 (2006).
10. C. Provenzano, P. Pagliusi, and G. Cipparrone, "Highly efficient liquid crystal based diffraction grating induced by polarization holograms at the aligning surfaces," Appl. Phys. Lett. **89**(12), 121105 (2006).
11. H. Sarkissian, S. V. Serak, N. Tabiryan, L. Glebov, V. Rotar, and B. Zeldovich, "Polarization-controlled switching between diffraction orders in transverse-periodically aligned nematic liquid crystals," Opt. Lett. **31**(15), 2248–2250 (2006).
12. S. Pancharatnam, "Achromatic combinations of birefringent plates. Part 1: An Achromatic Circular Polarizer," Proc. - Indian Acad. Sci. A **41**(4), 130–136 (1955).
13. M. Berry, "Quantal phase factors accompanying adiabatic changes," Proc. R. Soc. London, A **392**(1802), 45–57 (1984).

#297315 https://doi.org/10.1364/OE.25.019298
Journal © 2017 Received 2 Jun 2017; accepted 25 Jul 2017; published 1 Aug 2017

Optics EXPRESS


14. L. Marrucci, C. Manzo, and D. Paparo, "Pancharatnam-Berry phase optical elements for wavefront shaping in the visible domain: switchable helical modes generation," Appl. Phys. Lett. **88**, 221102 (2006).
15. J. Kim, Y. Li, M. N. Miskiewicz, C. Oh, M. W. Kudenov, and M. J. Escuti, "Fabrication of ideal geometric-phase holograms with arbitrary wavefronts," Optica **2**(11), 958–964 (2015).
16. B. Kress and T. Starner, "A review of head-mounted displays (HMD) technologies and applications for consumer electronics," Proc. SPIE **8720**, 87200A (2013).
17. T. Levola, "Diffractive optics for virtual reality displays," J. Soc. Inf. Disp. **14**(5), 467–475 (2006).
18. H. Kogelnik, "Coupled wave theory for thick hologram gratings," Bell System Technical Journal **48**(9), 2909–2947 (1969).
19. T. K. Gaylord and M. G. Moharam, "Thin and Thick gratings: terminology clarification," Appl. Opt. **20**(19), 3271–3273 (1981).
20. P. Ayras, P. Saarikko, and T. Levola, "Exit pupil expander with a large field of view based on diffractive optics," J. Soc. Inf. Disp. **17**(8), 659–666 (2009).
21. I. K. Baldry, J. B. Hawthorn, and J. G. Robertson, "Volume phase holographic gratings: polarization properties and diffraction efficiency," Publ.Astron.Soc.Pac. **116**(819), 403–414 (2004).
22. A. Shishido, "Rewritable holograms based on azobenzene-containing liquid-crystalline polymers," Polym. J. **42**, 525–533 (2010).
23. A. Bogdanov, A. Bobrovsky, A. Ryabchun, and A. Vorobiev, "Laser-induced holographic light scattering in a liquid-crystalline azobenzene-containing polymer," Phys. Rev. E **85**(1), 011704 (2012).
24. H. Ono, T. Sekiguchi, A. Emoto, and N. Kawatsuki, "Light wave propagation in polarization holograms formed in photoreactive polymer liquid crystals," Jpn. J. Appl. Phys. **47**(5), 3559–3563 (2008).
25. T. Sasaki, K. Miura, O. Hanaizumi, A. Emoto, and H. Ono, "Coupled-wave analysis of vector holograms: effects of modulation depth of anisotropic phase retardation," Appl. Opt. **49**(28), 5205–5211 (2010).
26. C. Oh and M. J. Escuti, "Achromatic diffraction from polarization gratings with high efficiency," Opt. Lett. **33**(20), 2287–2289 (2008).
27. R. K. Komanduri, K. F. Lawler, and M. J. Escuti, "Multi-twist retarders: broadband retardation control using self-aligning reactive liquid crystal layers," Opt. Express **21**(1), 404–420 (2013).
28. C. Oh and M. J. Escuti, "Numerical analysis of polarization gratings using the finite-difference time-domain method," Phys. Rev. A **76**(4), 043815 (2007).
29. R. K. Komanduri and M. J. Escuti, "Elastic continuum analysis of the liquid crystal polarization grating," Phys. Rev. E **76**(2), 021701 (2007).
30. M. Xu, D. K. G. de Boer, C. van Heesch, A. J. H. Wachters, and H. P. Urbach, "Photoanisotropic polarization gratings beyond the small recording angle regime," Opt. Express **18**(7), 6703–6721 (2010).
31. T. M. de Jong, D. K. G. de Boer, and C. W. M. Bastiaansen, "Surface-relief and polarization gratings for solar concentrators," Opt. Lett. **19**(16), 15127–15142 (2011).
32. H. Sarkissian, B. Park, N. Tabirian, and B. Zeldovich, "Periodically Aligned Liquid Crystal: Potential Application for Projection Displays," Mol. Cryst. Liquid Cryst. **451**, 1–19 (2006).
33. J. Chou, L. Parameswaran, B. Kimball, and M. Rothschild, "Electrically switchable diffractive waveplates with metasurface aligned liquid crystals," Opt. Express **24**, 24265–24273 (2016).
34. K. Gao, C. McGinty, H. Payson, S. Berry, J. Vornheim, V. Finnemeyer, B. Roberts, and P. Boss, "High-efficiency large-angle Pancharatnam phase deflector based on dual-twist design," Opt. Express **25**(6), 6283–6293 (2017).
35. M. J. Escuti, D. J. Kekas, and R. K. Komanduri, "Bragg liquid crystal polarization gratings," US Patent Application **14/813,660** (2014).
36. S. Kelly, "Anisotropic networks," J. Mater. Chem. **5**(12), 2047–2061 (1995).
37. D. J. Broer, "Photoinitiated polymerization and crosslinking of liquid-crystalline systems," in *Radiation Curing in Polymer Science and Technology, Volume 3: Polymerisation Mechanisms* (Springer, 1993), Ch. 12, pp. 383–443.
38. Y. Weng, D. Xu, Y. Zhang, X. Li, and S. T. Wu,"Polarization volume grating with high efficiency and large diffraction angle," Opt. Express **24**(15), 17746-17759 (2016).
39. J. Kobashi, H. Yoshida, and M. Ozaki, "Planar optics with patterned chiral liquid crystals," Nature Photon. **10**, 389âĂŞ392 (2016).
40. M. N. Miskiewicz and M. J. Escuti, "Optimization of direct-write polarization gratings," Opt. Eng. **54**(2), 025101–10 (2015).
41. L. De Sio, D. E. Roberts, Z. Liao, S. Nersisyan, O. Uskova, L. Wickboldt, N. Tabiryan, D. M. Steeves, and B. R. Kimball, "Digital polarization holography advancing geometrical phase optics," Opt. Express **24**(16), 18297–18306 (2016).
42. M. Schadt, K. Schmitt, V. Kozinkov, and V. Chigrinov, "Surface-induced parallel alignment of liquid crystals by linearly polymerized photopolymers," Jpn. J. Appl. Phys. **31**(7), 2155–2164 (1992).
43. V. Chigrinov, A. Muravski, H.-S. Kwok, H. Takada, H. Akiyama, and H. Takatsu,, "Anchoring properties of photoaligned azo-dye materials," Phys. Rev. E **68**(6), 061702–5 (2003).
44. E. A. Shteyner, A. K. Srivastava, V. G. Chigrinov, H.-S. Kwok, and A. D. Afanasyev, "Submicron-scale liquid crystal photo-alignment," Soft Matter **9**(21), 5160–5165 (2013).

Optics EXPRESS

## 1. Introduction

Polarization Gratings (PGs) are diffractive optical elements [1–3] comprising an in-plane anisotropy orientation that varies linearly along a surface, with a fixed anisotropy magnitude. They can be formed by azobenzene-containing polymers [1, 4], "form-birefringence" in isotropic materials via high frequency surface profiles [5, 6], plasmonic metasurfaces [7], and photo-aligned bulk liquid crystals (LCs) [8–11], and operate via the geometric phase [12–15]. It has been shown in theory and experiment that they manifest compelling optical properties at large periods, including high (100%) efficiency into a single order and strong polarization selectivity. However, no one has yet experimentally demonstrated efficiency approaching 100% when the period is near or below the wavelength, especially for visible lightwaves. If successfully realized, this would be a fundamentally new means for high efficiency at very large diffraction angles, with unique constraints and benefits for many applications, such as augmented-reality systems [16, 17], spectroscopy, optical telecommunications, polarimetry, front/back-lighting, nonmechanical beam steering, and remote optical sensing.

## 2. Background

Classical grating analysis [18, 19] distinguishes Raman-Nath (*thin*) from Bragg (*thick*) grating regimes, irrespective of materials and fabrication methods. A dimensionless parameter is often used to distinguish between them: $Q = 2\pi\lambda d/\bar{n}\Lambda^2$, where $\Lambda$, $\lambda$, $d$ and $\bar{n}$ are the period, vacuum wavelength, thickness, and average index, respectively. Traditionally, (isotropic) gratings in the Raman-Nath regime ($Q < 1$) have wide angular and spectral bandwidths, maximum single-order efficiency of less than 34%, and produce many diffraction orders. Conversely, those in the Bragg regime ($Q > 10$) have sharply selective angular and spectral response, and can produce up to 100% efficiency into a single order when the incident wave travels along the Bragg angle within the grating medium:

$$|\sin\theta_B| = \lambda/2\bar{n}\Lambda. \tag{1}$$

The most common gratings have been surface-relief-gratings [17, 20] (SRGs) and volume-holographic-gratings [21] (VHGs).

The earliest report of a Bragg PG was an experimental study [4] employing a azo-polymer with low birefringence $\Delta n$ ($\sim 0.01$), achieving $\geq 90\%$ diffraction efficiency, with $\Lambda = 2$ $\mu$m, $\lambda = 633$ nm, $d = 100$ $\mu$m, $\theta_B = 9.3°$, and $Q \approx 64$. However, smaller periods would require much thicker films, *e.g.*, $d = 1$ mm for $\Lambda = \lambda$ at the same $Q$, which is unfeasible due to the manifestation of haze and absorption [22, 23]. Subsequent prior art [24, 25] used numerical simulation and theoretical analysis to predict more generally that PG diffraction efficiency as high as 100% is possible in the Bragg regime for circularly polarized input and oblique incidence.

Nearly all prior art PGs fall into the Raman-Nath regime ($Q < 1$) when $\Lambda >> \lambda$. These PGs manifest high ($\sim 100\%$) first-order diffraction efficiencies [1, 8–10], either from a non-chiral uniaxially birefringent material with $d = \lambda/2\Delta n$, or alternatively, in certain combinations of multiple chiral LC layers [26, 27]. Some works [24, 28–31] examined PGs formed by a single bulk nematic LC layer as $\Lambda \sim \lambda$ when $Q \lesssim 1$. These studies concluded that high diffraction efficiency at large diffraction angles would require an unfeasibly high birefringence [28] (*i.e.*, $\Delta n > 0.4$), would be impossible due to degradation of the polarization interference during recording [30], and/or would face a critical thickness limitation [29, 32] ($\Lambda/2 \leq d_C < \Lambda$) beyond which the nematic LC cannot be directed into the PG pattern by alignment surfaces (*e.g.*, a PG with $Q = 10$ and $\Lambda = \lambda$ and $\bar{n} = 1.65$ requires $d = 2.6\Lambda$, which is $>> d_C$). Two recent experimental reports have found ways to partially overcome some of these limitations. In one, a switchable PG ($\Lambda = 900$ nm, $\lambda = 405$ nm, and $Q \approx 2$) was realized by aligning the LC with a metasurface [33], producing 35% peak efficiency. In another, a photo-aligned LC polymer PG ($\Lambda = 1$ $\mu$m, $\lambda = 633$ nm, and $Q \approx 6$) produced 90% peak efficiency [34].

Optics EXPRESS

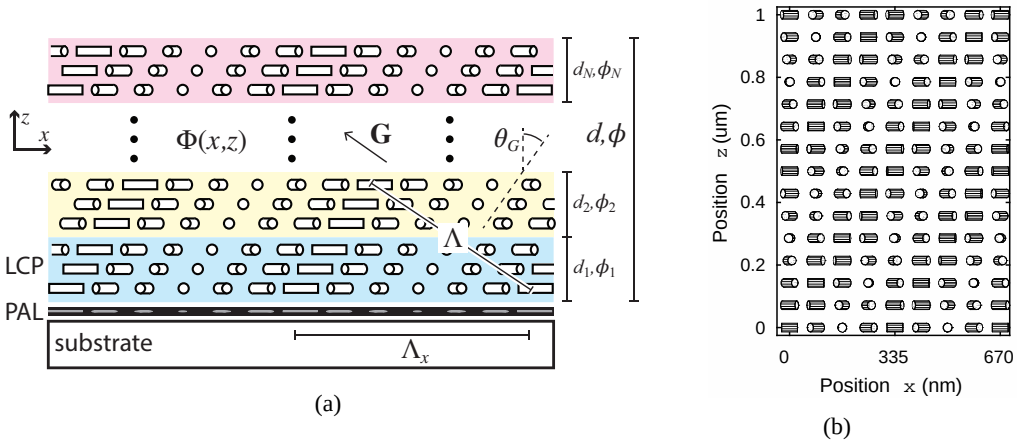


Fig. 1. LC polymer Bragg PG nematic director structure formed by $N$ sublayers: (a) illustrated schematic, and (b) calculated director orientations, with $\Lambda = 335$ nm, $\phi = -340°$, $d = 1000$ nm.

A few years ago, we outlined in a patent application [35] the concept and demonstration of building up the required LC thickness for a Bragg PG with high efficiency in the infrared via a plurality ($N$) bulk LC sublayers and a single alignment layer. We also introduced how to use chiral dopants to achieve a grating slant. We employed reactive mesogens [36, 37], also called a low-molecular weight LC polymer (LCP) network, wherein the thickness $d_i$ ($i = 1..N$) of each sublayer was thinner than $d_C$. More recently, and apparently independently, a purely simulation-based study [38] examined a similar type of slanted bulk LC Bragg PG for transmissive cases when $\Lambda > \lambda$, which they called a polarization volume grating.

In this paper, we detail experimental results of Bragg PGs formed in bulk LCs with near-100% first-order efficiency at a blue wavelength with a subwavelength period. We also show how to control the slant angle to achieve on-axis peak efficiency, and characterize for the first time the polarization and spectrum of the diffracted orders.

## 3. Definitions and fundamental properties

The periodic structure of both switchable and polymerized LC PGs is embodied in the orientation of its optic axis (*i.e.*, nematic director), where $d$ is constant. The in-plane orientation angle $\Phi$ may vary both along the surface $x$ and the thickness $z$, when a chiral nematic material is employed [26, 27, 38, 39]:

$$\Phi(x, z) = \pi x/\Lambda_x + \phi z/d, \tag{2}$$

where $\phi$ is the twist angle of the layer and $\Lambda_x$ is the period at the surface (Fig. 1(a)). In Fig. 1(b) we show the calculated director profile using Eq. (2) for the parameters corresponding to the 3% chiral sample discussed below. This nematic director profile may be seen as a planar cholesteric structure with a vertical helix axis, but wherein the start angle of the helix varies linearly along the in-plane direction. It is exactly this in-plane variation that generates the gradient phase, *i.e.*, diffraction, and it is the chiral twist that generates the grating slant. In this present work, nearly all $(d_i, \phi_i)$ are identical, except for the optically negligible first sublayer. However, the reader should note that each sublayer has the potential to be individually controlled; this enables a wide design-space that allows for the fine tuning of optical characteristics for various applications, a topic for future work. Nevertheless, our focus here is on the fundamental properties of the

Optics EXPRESS

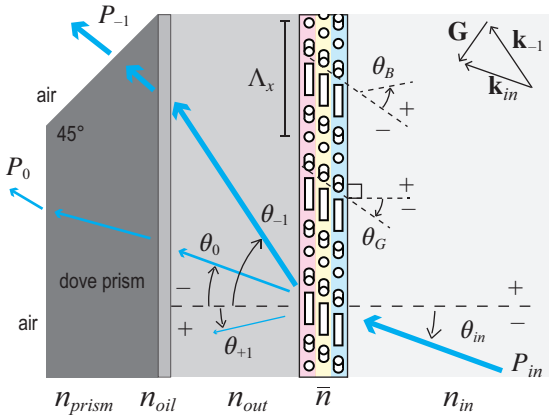


Fig. 2. LC polymer Bragg PG measurement notation.

simplest grating, *i.e.*, one with at most a single slant. The slant angle $\theta_G$ is

$$\tan\theta_G = \phi\Lambda_x/d\pi. \tag{3}$$

The peak efficiency angle of incidence $\theta_P$ is related to the slant angle by the equation

$$\sin(\sin^{-1}((n_{in}/\bar{n})\sin\theta_P) - \theta_G) = \sin\theta_B, \tag{4}$$

where $n_{in}$ is the refractive index of the incident medium. For unslanted gratings ($\theta_G = 0$), peak diffraction efficiency occurs when the angle of incidence $\theta_{in} = \theta_P = \theta_B$.

The pattern $\Phi(x, 0)$ may be formed via holographic lithography [8–10, 15], direct-write laser scanning [15, 40], or digital projection lithography [41]. Note that the recording process always sets $\Lambda_x$ in the photo-alignment [42, 43] layer (PAL), and that the volumetric period depends on this *and* the slant angle ($\Lambda = \Lambda_x \cos\theta_G$). Two consequences of this can be uncovered by considering the conservation of momentum [18] ($\mathbf{k}_m = m\mathbf{G} + \mathbf{k}_{in}$), illustrated in Fig. 2. First, unlike slanted VHGs [21], all slanted LC Bragg PGs with the same $\Lambda_x$ will diffract into the same output angles. Second, the diffraction angle $\theta_m$ for order $m$ (for PGs in any regime) follows:

$$n_{out}\sin\theta_m = m\lambda/\Lambda_x + n_{in}\sin\theta_{in}, \tag{5}$$

where $n_{out}$ is the exit media refractive index. Our angle convention is shown in Fig. 2. For ideal PGs, only the first and zero diffraction orders [15], $m = \{-1, 0, +1\}$, can have non-zero efficiency.

## 4. Fabrication

Here, we aim to fabricate a series of LC polymer Bragg PGs with $\Lambda = 335$ nm for $\lambda = 450$ nm, where we vary the chiral material concentration to adjust $\phi$ and $\theta_G$.

Fabrication begins with coating the azo-based PAL [43] LIA-CO01 (DIC Corp) on clean glass (D263) substrates (spin: 30 s @ 1500 rpm, bake: 60 s @ 130°C), about 30 nm thick. For exposure, we employ two-beam polarization holographic lithography [8, 9], using a solid-state 355 nm laser (Coherent Inc) arranged to provide two coherent, orthogonal, circularly polarized beams superimposed onto the PAL at ±32°. Exposure energy was 4 J/cm$^2$. The first LCP sublayer we coat serves the purpose of extending and enhancing the anchoring strength of the PAL to the second LCP sublayer. We use a first reactive mesogen solution, comprising solids RMM-A (Merck KGaA, $\Delta n = 0.17$ @ 450 nm) in solvent propylene-glycol-methyl-ether-acetate (PGMEA from Sigma-Aldrich), with a 5% solids concentration. This is processed (spin: 60 s @

Optics EXPRESS

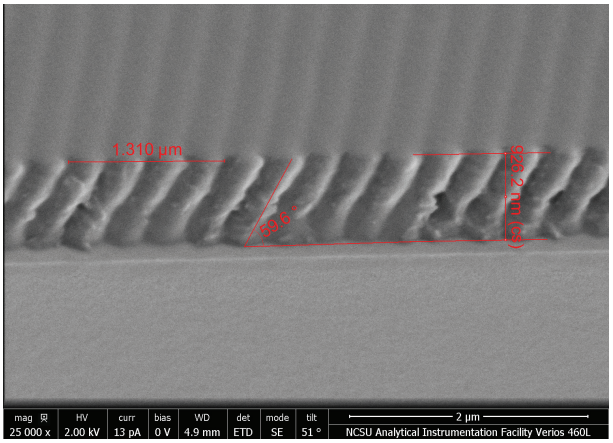


Fig. 3. Scanning electron microscope image of a slanted Bragg PG (3% chiral) with peak efficiency angle $\theta_P = -3°$.

700 rpm, cure: 30 s @ 190 mW of UV illumination from a 365 nm LED in dry nitrogen environment) to create approximately $d_1 = 75$ nm and $\phi_1 = 0$. The next set of sublayers cause nearly all of the diffraction. For the second and subsequent sublayers, we use a second reactive mesogen solution, comprising 3% RMM-B (Merck KGaA, $\Delta n = 0.28$ and $\bar{n} = 1.68$ @ 450 nm) in solvent PGMEA and in most cases a chiral nematic reactive mesogen RMM-C (Merck KGaA, helical pitch ~ 400 nm and $HTP \sim 2.5\ \mu\text{m}^{-1}$, otherwise identical to RMM-B). This is processed (spin and cure steps identical to the first LCP sublayer except for 1000 rpm) to create $d_2 = 55$ nm. This was repeated 16 times, for a total of $N = 18$ and approximately $d = 1000$ nm. Thicknesses were measured by profilometer and ellipsometer.

To facilitate the the diffraction efficiency measurement for a wide range of incidence angles accurately, we laminated a high index substrate ($n_{out} = 1.74$) onto the grating ($\bar{n} = 1.68$ @ 450 nm) with optical glue (NOA 170, Norland Products, Inc). The first diffraction order is then out-coupled with high index oil ($n_{oil} \approx 1.7$) and a Dove prism made from SF11 glass ($n_{prism} = 1.82$). The original glass substrate (D263) will then serve as an endcap ($n_{endcap} = 1.53$).

## 5. Results

To examine the nanoscale nematic director profile of the LCP, we prepared one sample with 3% chiral concentration for study with a scanning electron microscope (SEM). We first submersed it in liquid nitrogen, then broke it, and finally evaporated a 5 nm layer of gold onto it. The resulting cross-section of the fractured edge is shown in Fig. 3, from the same perspective as Fig. 1. The overall structure corresponds well to the expected nematic director profile of Eq. (2), where both the periodicity and grating slant are easily observed. The period and film thickness measured by the SEM software corresponds well to our other measurements. The SEM-measured slant angle is around $-30°$ (including the negative sign to be consistent with the coordinates), which can be used along with Eq. (4) to predict a peak efficiency angle $\theta_P \approx -3°$. This also shows good agreement with the optically measured value for this slant (*i.e.*, purple curves discussed next), and with the nematic director predicted in Fig. 1(b). This same grating texture was observed over the entire 10 mm long edge of our SEM sample.

A series of LC polymer Bragg PGs were fabricated using a range of chiral concentrations, from 0% to 6%, in order to achieve different peak diffraction angles. The nonchiral sample (blue) is shown in Fig. 4 with a peak first-order efficiency of about 99%, defined as $\eta_{-1} = P_{-1}/(P_{-1} + P_0)$ where $P_m$ is the output power of order $m$. Its corresponding field-of-view $FOV$

Optics EXPRESS

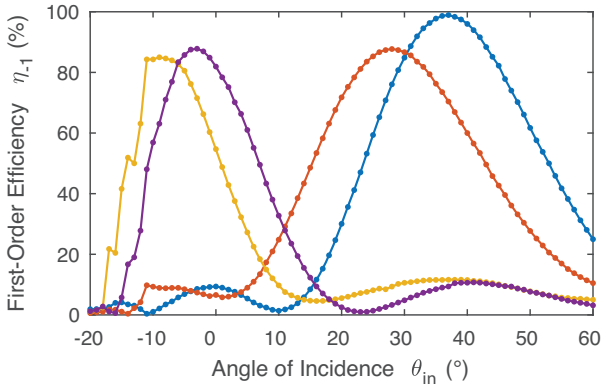


Fig. 4. Measured angular response of the diffraction efficiency of several LC polymer Bragg PGs, all with $\Lambda_x = 335$ nm, at $\lambda = 450$ nm, circular input polarization, and various slant angles. Chiral concentrations: 0%=blue, 1%=red, 3%=purple, 6%=yellow.

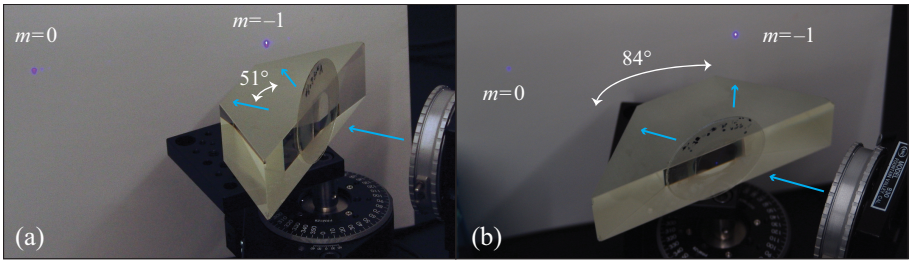


Fig. 5. Photographs of the samples corresponding to the (a) chiral (purple) and (b) nonchiral (blue) curves, respectively. In both, the deflection angle between the zero- and first-orders is indicated in (a) the high-index substrate before the prism, and (b) in air without the prism.

was 29°, defined as the full-width-half-max (FWHM) of the angular response. As chiral material is incorporated, the slant angle becomes nonzero and the peak angle shifts toward negative angles, as anticipated by Eq. (4), eventually meeting and exceeding the normal direction. These angular responses are also shown in Fig. 4. One sample (purple, 3% chiral) was nearly on-axis, with $\theta_P = -3°$, $\eta_{-1} = 88\%$, and $FOV = 19°$. A photograph of these two samples at peak diffraction is also shown in Fig. 5(a) and 5(b). The general trends are summarized in Fig. 6, where $\eta_{-1}$, $FOV$, and $\Lambda$ decrease slightly, while $\theta_G$ and $\phi$ decrease substantially, all in a linear fashion with respect to $\theta_P$.

We also measured the spectral response of the zero-order for two samples with a spectrophotometer, and estimated the first-order efficiency. The result is shown in Fig. 7, where we observe the remarkably wide spectral bandwdith (FWHM) of $\geq 200$ nm.

Two polarization measurements were performed. First, we measured the zero- and first-order efficiencies as the incident polarization was varied by rotating a quartz quarterwave (QW) plate receiving linearly polarized light, to vary the input from circular to linear and back to the orthogonal circular polarization. The result is shown in Fig. 8(a) for the nonchiral and nearly on-axis samples (blue and purple results in Fig. 4). The response shows that for both nonchiral and chiral Bragg PGs the highest and lowest efficiencies occur for left- and right-handed circular (LHC, RHC) input polarizations, respectively, as anticipated [4, 24, 25, 35]. It is notable that when the input is RHC, the Bragg PG is nearly transparent. The extinction ratio of the first-order for LHC/RHC input is about 400:1 and 55:1 for the nonchiral (blue) and chiral (purple) samples,

Optics EXPRESS

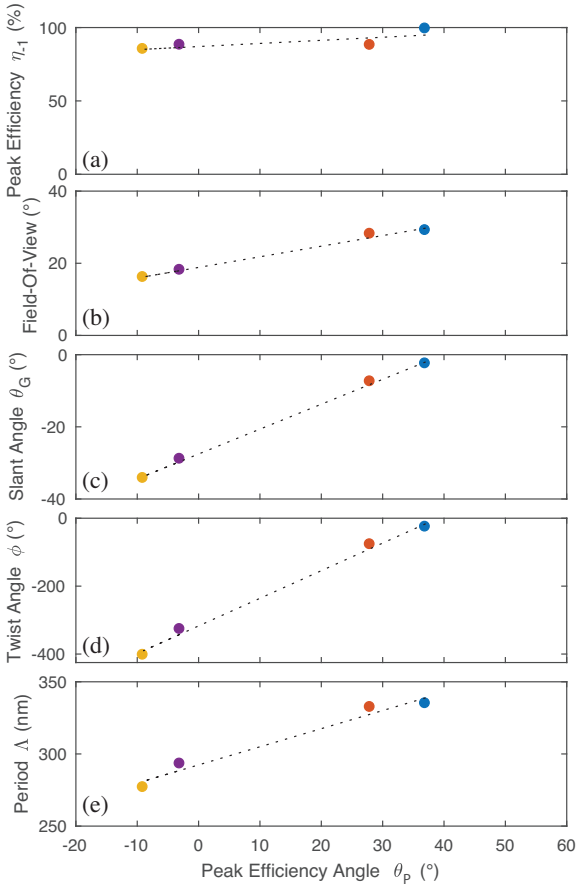


Fig. 6. Measured properties of several LC polymer Bragg PGs: (a) $\eta_{-1}$, (b) $FOV$, (c) $\theta_G$, (d) $\phi$, and (e) $\Lambda$. Colors correspond to the curves and chiral concentrations in Fig. 4.

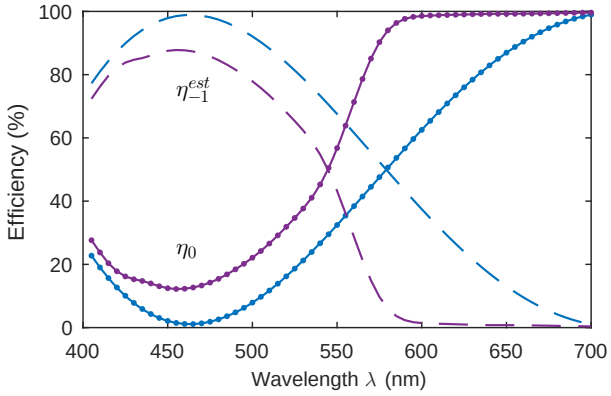


Fig. 7. Spectral response of two LC polymer Bragg PGs, nonchiral (blue) and 3% chiral (purple). The $\eta_0$ curve was measured and used to estimate $\eta_{-1}^{est} = 100 - \eta_0$.

respectively. Second, we measured the output polarization states of the zero- and first-orders when the input polarization was set to achieve maximum efficiency. The result for these same

Optics EXPRESS

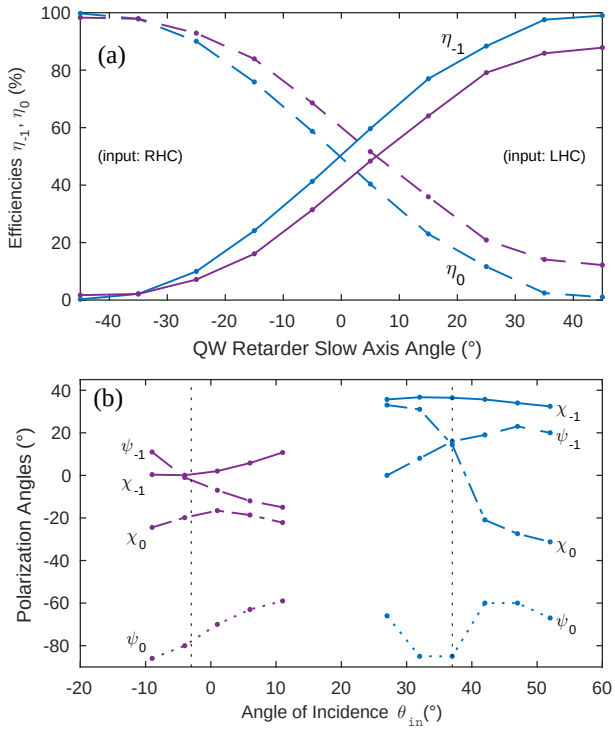


Fig. 8. Measured polarization response of two LC polymer Bragg PGs, nonchiral (blue) and 3% chiral (purple): (a) efficiencies as input polarization is varied by rotating a quarterwave (QW), and (b) output polarization angles (orientation $\psi$, ellipticity $\chi$) of both orders in Fig. 5.

two samples across their respective *FOV* is shown in Fig. 8(b). As expected, the first-order handedness (RH) is also opposite the input LHC. Most notably, the nonchiral sample (blue) output a first-order with nearly circular polarization (ellipticity angle $\chi_1 \sim 40°$). Somewhat most surprisingly, the chiral sample (purple) output a nearly linearly polarized first-order. In both cases, the zero-orders are elliptically polarized.

Finally, we measured what occurs when total-internal-reflection (TIR) causes the first-order to reflect back onto the same grating multiple times. We illustrate in Fig. 9 the light path and the measured efficiencies of each interaction, relative to the input. After the first interaction, 88% of the incident wave was directed into a waveguiding angle, with nearly linear polarization. After TIR at the waveguide-air surface and returning for the second set of interactions, most of the light undergoes TIR at the endcap, and is equally split into its zero- and first-orders, where 41% diffracts out ($m = +1$ order). This apparently occurs because the two TIR events preserved the linear polarization of the wave. The remaining interactions out-couple a lower and lower fraction of the light, presumably because each adjusts the polarization.

## 6. Discussion

We selected this set of $\Lambda$ and $\lambda$ because blue is the most extreme visible color of a light-emitting-diode or laser light source, and also because this challenging sub-wavelength period is especially relevant to exit-pupil-expanders [17, 20] (EPE) based on diffractive waveguides. All larger periods/wavelengths should be easier to realize. The unslanted version of this grating should have $\theta_B = 42°$ in air, meaning that light incident at this angle will diffract into $\theta_{-1} = -42°$ when

Optics EXPRESS

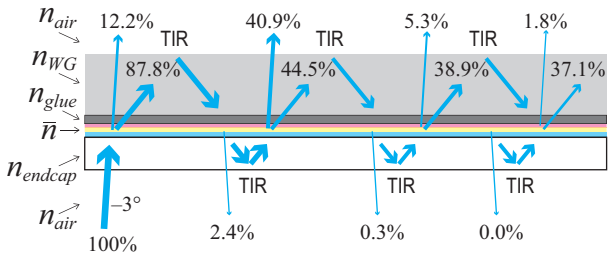


Fig. 9. Measured efficiencies for a slanted (purple) LC polymer Bragg PG when TIR of the first-order wave leads to waveguiding and multiple interactions.

both $n_{in} = n_{out} = 1$, a remarkable 84° deflection angle (between the zero- and first-orders). At normal incidence, the (on-axis) slanted version of this grating will diffract into $\theta_{-1} = 50.5°$ inside a high index ($n_{out} = 1.74$) substrate, according to Eq. (5). In order to experimentally verify Eq. (5), we measured the output diffraction angle at the peak angle incidence ($\theta_{in} = \theta_P = -3°$) in the 3% chiral sample, and found that $\theta_{-1} \approx 45°$ inside the exit medium (waveguide), which is very close to the analytic prediction $\theta_{-1} = 45.2°$. These PGs are solidly in the Bragg regime ($Q \approx 17$) and $\Lambda_x$ is nearly 3000 lines/mm for all samples. Both unslanted and slanted Bragg PGs reach the maximum efficiency around half-wave thickness [38], which is similar to conventional Raman-Nath PGs [1, 2, 28].

Interestingly, these LC polymer Bragg PGs employ a relatively-high $\Delta n$ and therefore $d$ is lower than VHGs [21]. This leads to a much larger $FOV$ and spectral bandwidth while maintaining high efficiency. As compared to SRGs, the efficiency and $FOV$ are comparable, or even moderately larger [20]; nevertheless, a primary benefit may be the absence of development and etching steps in fabrication. Note that because the twist and thickness of each sublayer in LC polymer Bragg PGs can be independently adjusted, it should be possible to implement structures more complex than the single slant described here; for example, two slants to increase the FOV.

The transmittance, defined as $T_m = P_m/P_{in}$, is nearly the same efficiency in our case, because the primary loss is the air-glass interfaces (about 5% each), and lower losses between the various glass, glue, and oil media (see Fig. 2). There was no haze observable by eye, and the absorbance of the LCP and PAL materials at 450 nm is < 1%.

This work uncovers several surprises. First, while the input polarization response [Fig. 8(a)] is the same as Raman-Nath PGs, the output polarization [Fig. 8(b)] is unexpected: (i) it is not guaranteed to be circular, as in Raman-Nath PGs; and (ii) when the grating has a substantial slant, it is in general complex (depending at least on $\theta_{in}, \phi$), and is sometimes almost purely linear. Second, it may be surprising to some that photo-alignment layers might support grating periods so small – nevertheless, at least one prior report [44] showed limited diffraction down to 200 nm periods. Third, a nonchiral material can apparently lead to $\theta_P$ (= 38°) slightly less than predicted $\theta_B$ (= 42°), *i.e.*, blue curve in Fig. 4. Note we have repeatedly checked our period and angular response measurements; we also do not observe this behavior in our other work at $\Lambda_x \geq 400$ nm. This effect may be related to the appearance of pretilt in this nonchiral case.

## 7. Conclusion

We experimentally demonstrated the first LC polymer Bragg PGs at a visible wavelength ($\lambda = 450$ nm) and sub-wavelength period ($\Lambda_x = 335$ nm) — the smallest for a high-efficiency PG of any kind. We assessed the use of a chiral nematic twisted LC material to achieve a slanted grating, and thereby adjust the angle of peak efficiency on-axis. These LC Bragg PGs manifest nearly ideal properties, including 85-99% efficiency, 19-29° $FOV$, and have a spec-

Optics EXPRESS

tral bandwidth of about 200 nm. They are strongly selective to input polarization, but in some cases produce unexpected output polarization. We believe the path is now viable for PGs development into many new small-period/large-angle applications, including augmented-reality systems, spectroscopy, optical telecommunications, polarimetry, front/back-lighting, nonmechanical beam steering, and remote optical sensing.

## Funding

ImagineOptix Corporation (NCSU grant #2014-2450)

## Acknowledgments

We thank Shuojia Shi and Tatsuya Hirai for assistance in fabrication development and Merck KGaA for customized materials. We also thank Chuck Mooney at the NCSU Analytical Instrumentation Facility for the electron microscopy. MJE holds an equity interest in ImagineOptix Corp.